Mineral-Inspired Crystal Growth and Physical Properties of Na 2 Cu(SO 4) 2 and Review of Na 2 M (SO 4) 2 (H 2 O) x (x = 0–6) Compounds

Vadim M Kovrugin, Diana O Nekrasova, Oleg I Siidra, Olivier Mentre, Christian Masquelier, Sergey Yu. Stefanovich, Marie Colmont

Mineral-Inspired Crystal Growth and Physical Properties of $Na_2Cu(SO_4)_2$ and Review of $Na_2M(SO_4)_2(H_2O)_x$ (x = 0−6) Compounds

Vadim M. Kovrugin,[*,†,‡] Diana O. Nekrasova,[†,§] Oleg I. Siidra,[*,†,∥] Olivier Mentré,[§] Christian Masquelier,[‡] Sergey Yu. Stefanovich,[⊥] and Marie Colmont[§]

[†]Department of Crystallography, St. Petersburg University, 199034 St. Petersburg, Russia

[‡]Laboratoire de Réactivité et de Chimie des Solides (LRCS), UMR 7314, Université de Picardie Jules Verne, 80039 Amiens Cedex, France

[§]Unité de Catalyse et Chimie du Solide (UCCS), UMR 8181, Université Lille 1, 59655 Villeneuve d'ASCQ, France

[∥]Nanomaterials Research Center, Kola Science Center, Russian Academy of Sciences, Apatity, Murmansk Region 184200, Russia

[⊥]Department of Chemistry, Moscow State University, Leninskie Gory 1, 119991 Moscow, Russia

ABSTRACT: Single crystals and polycrystalline samples of a synthetic analogue of saranchinaite, $Na_2Cu(SO_4)_2$, have been prepared by two different methods. The structural analysis revealed unusual heptahedral CuO_7 coordination [4 + 1 + 2] of Cu^{2+} cations in its crystal structure. The title compound crystallizes in the noncentrosymmetric space group $P2_1$ and exhibits the averaged nonlinear coefficient $\langle d \rangle = 1.4[d_{14}(SiO_2)] \approx 0.5$ pm/V. Electrochemical tests showed a limited electrochemical performance and low mobility of Na ions in the structure. The magnetic properties of $Na_2Cu(SO_4)_2$ reflect its crystal structure with half of copper cations as mainly paramagnetic and the other half as strongly engaged in antiferromagnetic dimer interactions. Analysis of the synthesis methods for preparation of the other Na-containing anhydrous sulfates is reported. Dehydration of the $Na_2M(SO_4)_2(H_2O)_x$ (x = 0−6) phases, various structure types, and the structural complexity of $Na_2M(SO_4)_2$ (M = Mn, Co, Ni, Cu, Zn, Cd) compounds are also discussed.

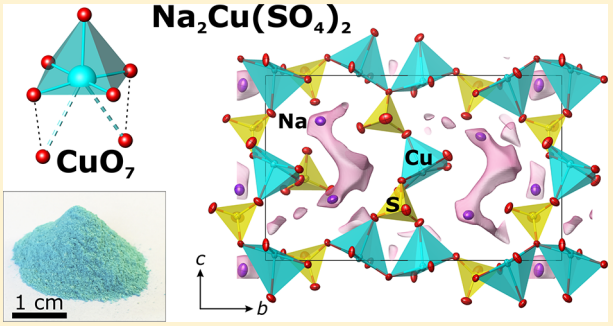

INTRODUCTION

Mineralogy has always provided an inspiration for finding new materials with useful properties.[1−3] Nowadays, the experimental mineralogy of sulfates is experiencing a renaissance due to their geochemical abundance in nature on Earth and recent discoveries of significant amount of sulfates on the surface of Mars.[4,5] Synthetic sulfate compounds are also of special interest from the viewpoint of exhibiting promising physical properties. For example, novel polyanionic materials with high voltage potential of electrodes can be fabricated by substituting a phosphate anion by a sulfate anion,[6−11] thus taking advantage of the higher electronegativity of SO_4 groups.[12] Indeed, the mineral-inspired eldfellite-type $NaFe(SO_4)_2$ phase has been recently considered as a low-cost cathode in a rechargeable Na ion battery, demonstrating about 80 mAh/g of reversible capacity with a discharge voltage of 3.0 V vs Na^+/Na for a relatively long life.[13−16] However, we should note that most anhydrous sulfates are unstable under ambient conditions and are easily hydrated. This fact as well as complicated synthesis methods make them difficult for investigation. In contrast, the hydrated sulfates have been shown to be earth-abundant mineral species and can be relatively easily prepared in a laboratory. Though several works devoted to the investigation of electrochemical behavior of the kröhnkite type, $Na_2Fe(SO_4)_2(H_2O)_2$,[17−20] and blödite type, $Na_2M(SO_4)_2(H_2O)_4$ (M = Mg, Fe, Co, Ni, Zn),[21] compositions have been reported so far, the electrochemical performance (reversible discharge capacities less than ∼80 mAh/g) is worse than that of anhydrous sulfates. Taking into account structural linkages between hydrated and anhydrous sulfates,[22] the hydrates can be used as precursors for syntheses of anhydrous compositions.[23,24] Herein, we further explore this avenue and turn our mind to investigation of crystal growth and crystal chemistry of anhydrous and hydrated mineral-inspired transition-metal sulfates. Recent studies have demonstrated that the design of synthetic analogues of mineral-inspired phases may offer new, uncommon information and deep insight into aspects of crystal structure and crystal growth.[25−27] On the basis of all these considerations, we report on the synthesis of the synthetic analogue of the recently reported exhalative mineral saranchinaite,[28] $Na_2Cu(SO_4)_2$, discuss its structural, optical, thermal, electrochemical, and magnetic properties for the first

time, and review various structure types in a series of $Na_2M(SO_4)_2$ (M = Mn, Co, Ni, Cu, Zn, Cd) compositions.

EXPERIMENTAL SECTION

Single-Crystal Growth. By analogy with a formation of saranchinaite as a result of high-temperature exhalative processes occurring in the fumarole fields of Tolbachik volcano,[28] single crystals of $Na_2Cu(SO_4)_2$ were grown by slow cooling of a melt containing equimolar quantities of anhydrous $CuSO_4$ (Prolabo, 98%) and Na_2SO_4 (Alfa Aesar, 99%). As reported in our previous works, this method has appeared to resemble crystal growth processes from volcanic gases.[26,29,30] Precursors were predried at 100 °C for 2 h and further rapidly mixed and ground in an agate mortar in air for 5 min. The reaction mixture of precursors was loaded into a quartz ampule (ca. 15 × 0.9 cm), which was evacuated (10^{-2} mbar) and further sealed. The ampule was placed horizontally in a tubular furnace and heated to 950 °C at a rate of 230 °C/h and further held at this temperature for 72 h to produce a blue homogeneous melt. Then it was slowly cooled at a rate of 12.5 °C/h to 650 °C and further held for 24 h more. Finally, the furnace was slowly cooled to room temperature at a rate of 13.0 °C/h. The resulting solid products in the evacuated ampule are shown in Figure 1a.

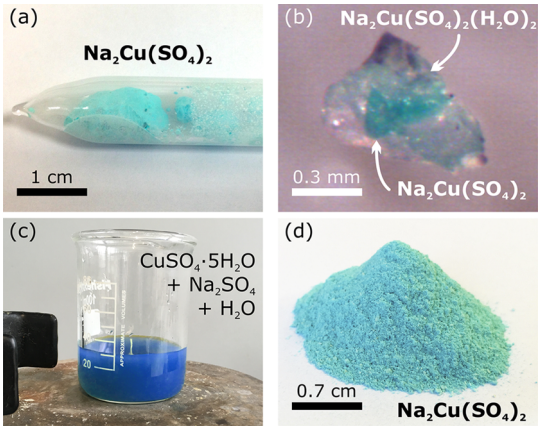

Figure 1. Evacuated ampule with $Na_2Cu(SO_4)_2$ (a), single crystal of $Na_2Cu(SO_4)_2$ in kröhnkite-based matrix (b), homogeneous aqueous precursor for $Na_2Cu(SO_4)_2$ (c), and pure powder sample of $Na_2Cu(SO_4)_2$ (d).

The as-prepared $Na_2Cu(SO_4)_2$ is sensitive to air moisture and starts to transform to the hydrated kröhnkite-type $Na_2Cu(SO_4)_2(H_2O)_2$ composition after 12 h of exposure to air, which is accompanied by a color change to a pale blue material. Single crystals of $Na_2Cu(SO_4)_2$ in a crystalline matrix of $Na_2Cu(SO_4)_2(H_2O)_2$ are shown in Figure 1b. Note that the observed hydration process is reversible, and the solids may be easily dehydrated by heating of the crystalline sample to 300 °C for 2 h.

Polycrystalline Sample Preparation. Powder samples of $Na_2Cu(SO_4)_2$ were prepared by a coprecipitation-type synthesis process. $CuSO_4·5H_2O$ (Sigma-Aldrich, ≥99.0%) and Na_2SO_4 (Alfa Aesar, 99%) were used as starting materials, while distilled water was used as solvent. The starting precursors taken in a 1.2:1.0 (=$CuSO_4·5H_2O$:Na_2SO_4) ratio were completely dissolved in water with vigorous magnetic stirring at room temperature in two steps. The speed of rotation was maintained at 300 rpm during the reaction. First, sodium sulfate was dissolved in water for 15 min. Then copper sulfate pentahydrate was added, and it was dissolved for the same time period until the solution became a homogeneous bright blue color (Figure 1c). Afterward, the solution of the reactants was heated to 110 °C for 5 h until evaporation. The resulting powder with a light blue color contains both saranchiniate-type $Na_2Cu(SO_4)_2$ and kröhnkite-type $Na_2Cu(SO_4)_2(H_2O)_2$ phases, as identified by powder X-ray diffraction analysis. Finally, the obtained mixture was heated to 300 °C for 2 h to produce a polycrystalline sample of anhydrous $Na_2Cu(SO_4)_2$ (Figure 1d). A high-purity (99%) sample was confirmed by X-ray powder diffraction analysis. Note, however, that there were several small peaks of an unidentified impurity, as illustrated in Figure 2 (inset).

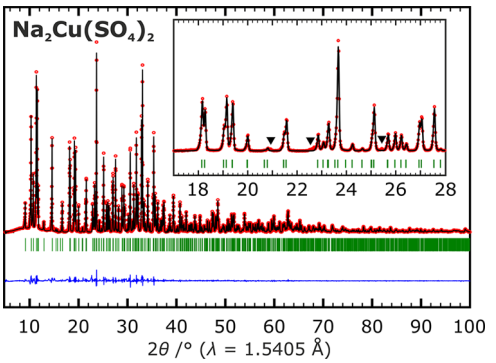

Figure 2. Results of the profile-matching analysis of $Na_2Cu(SO_4)_2$ from the powder XRD data. Impurities are shown by black triangles.

The equimolar amounts of starting precursors resulted in a preparation of $Na_2Cu(SO_4)_2$ with a small amount of Na_2SO_4 as an admixture. The probable hydration of starting precursors may serve as an explanation for the observed impurity of sodium sulfate.

The as-prepared powder sample of $Na_2Cu(SO_4)_2$ is less sensitive to air moisture in comparison to the crystals grown in an evacuated ampule. Hence, the powder is stable in air for about 2 days. To prevent further hydration, the sample should be kept in an oven at 100 °C or in a glovebox.

Single-Crystal X-ray Diffraction. Single crystals of $Na_2Cu(SO_4)_2$ selected for X-ray diffraction (XRD) data collection were mounted on thin glass fibers and tested on a Bruker APEX II DUO X-ray diffractometer with a Mo IμS microfocus X-ray tube (λ = 0.71073 Å) operated at 50 kV and 0.6 mA. More than a hemisphere of three-dimensional XRD data was collected with a frame width of 0.5° in ω and a 35 s count time for each frame. Then the collected data were integrated and corrected for absorption using a multiscan type model using Bruker software. Initial atomic coordinates for the crystal structure of synthetic $Na_2Cu(SO_4)_2$ were taken from the structure of the previously reported mineral phase.[28] The crystal structure was further refined in the noncentrosymmetric $P2_1$ space group to R_1 = 0.020 (wR_2 = 0.044) for 6263 reflections with $|F_o| \geq 4\sigma F$ by using the SHELXL program implemented in the WinGX program package.[31] The main crystallographic information for the synthetic and mineral phases is summarized in Table 1. Selected interatomic distances and results of bond valence calculations for Cu^{2+} are given in Table 2. Fractional atomic coordinates, atomic displacement parameters, and a comparison of Na−O bonds in the structures of synthetic and mineral phases are given in Tables S1−S3 in the Supporting Information. CCDC-1866049 (CSD, Cambridge) contains the supplementary crystallographic information for synthetic $Na_2Cu(SO_4)_2$.

Powder X-ray Diffraction. Routine powder XRD analyses of the samples were performed at room temperature using a D8 Advance Bruker diffractometer (Cu Kα radiation, λ = 1.5405 Å), with a step width of 0.02°. A high-quality XRD pattern used for profile matching analysis was recorded in the 2θ range of 5−100° with a step size of 0.01° using a Rigaku Smartlab diffractometer equipped with a 9 kW rotating anode. The profile matching analysis was carried out in the JANA2006 crystallographic system.[32] The background was fitted using a Chebyshev polynomial function, and the peak shapes were described by a pseudo-Voigt function. The refined unit-cell parameters in the space group $P2_1$ are a = 8.9655(1) Å, b = 15.5366(1) Å, c = 10.1384(1) Å, β = 107.07(1)°, and V = 1350(1) Å^3. The final observed, calculated, and difference powder XRD patterns resulting from the profile-matching procedure are plotted in Figure 2.

Table 1. Single-Crystal and Structure Refinement Data for Synthetic $Na_2Cu(SO_4)_2$ and Its "Natural" Analogue Saranchinaite[28]

	$Na_2Cu(SO_4)_2$	$(Na,K)_2Cu(SO_4)_2$[28]
Crystal Data		
space group	$P2_1$	$P2_1$
a (Å)	8.9711(3)	9.0109(5)
b (Å)	15.5482(5)	15.5355(8)
c (Å)	10.1421(3)	10.1507(5)
β (deg)	107.155(1)	107.079(2)
V (Å^3)	1351.73(7)	1367.06(12)
Z	2	2
ρ_{calc} (g cm^{-3})	2.964	2.970
μ (mm^{-1})	3.987	3.982
Data Collection		
$F(000)$	1176	1181
θ range (deg)	2.1−31.6	2.1−22.7
hkl limits	−13 → +13	−9 → +9
	−15 → +22	−16 → +16
	−14 → +14	−11 → +11
total no. of rflns	16018	10024
no. of unique rflns (R_{int})	6585 (0.0238)	3642 (0.0394)
no. of unique rflns, $F > 4\sigma F$	6263	3236
Refinement		
R_1 ($F > 4\sigma F$), wR_2 ($F > 4\sigma F$)	0.0204, 0.0436	0.0295, 0.0580
R_1 (all), wR_2 (all)	0.0224, 0.0443	0.0381, 0.0610
GOF	1.009	0.965
$\Delta\rho_{max}$, $\Delta\rho_{min}$ (e Å^{-3})	0.549, −0.437	0.459, −0.465

Infrared Spectroscopy (FTIR). The infrared (IR) spectrum (Figure 3a) of polycrystalline $Na_2Cu(SO_4)_2$ was measured using a PerkinElmer Spectrum Two FTIR spectrometer equipped with a diamond attenuated total reflectance (ATR) accessory with a resolution of 4 cm^{-1} and 16 scans. Absorption bands in the IR spectrum of $Na_2Cu(SO_4)_2$ and their assignments are as follows (cm^{-1}): 1248−955 (ν_4 S−O stretching vibrations), 684−605 (ν_1 and ν_3 S−O bending vibrations), 520 (ν Cu−O stretching vibrations). The splitting of all bands in the range 900−1250 cm^{-1} is due to the presence of eight symmetrically independent $(SO_4)^{2-}$ anions with a distorted-tetrahedral geometry. The band assignments were done according to refs 33−39. Note that after several hours of exposure to open air, $Na_2Cu(SO_4)_2$ starts to hydrate with the appearance of an intense band at 860 cm^{-1} (Cu···O−H bending vibrations).

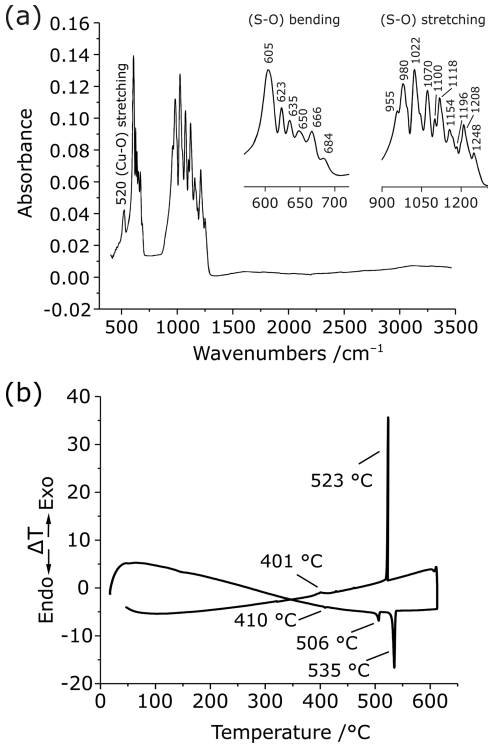

Figure 3. Infrared (FTIR) spectrum (a) and DTA curves (b) for $Na_2Cu(SO_4)_2$.

Thermal Analysis (DTA). Differential thermal analysis was done on a TGA 92 SETARAM instrument in an air atmosphere with a heating rate of 5 °C min^{-1} from room temperature up to 630 °C and the reverse (Figure 3b). Thermal evolution of synthetic $Na_2Cu(SO_4)_2$ occurs in three steps upon heating. The observed thermal phenomena are consistent with the temperature values of the phase transformations for the natural phase (mineral) determined recently by our high-temperature powder XRD (HTPXRD) study.[28] Thus, the powder XRD patterns collected for the mineral $(Na,K)_2Cu(SO_4)_2$ phase (Figure S1) were used for further comparative thermal analysis. The first small endothermic peak centered at 410 °C is related to the

Table 2. Cu−O Bond Lengths (in Å) and Bond Valence Sums in Brackets (in Valence Units, vu) in the Structures of Synthetic $Na_2Cu(SO_4)_2$ and Its "Natural" Analogue Saranchinaite[28] [a]

atoms	$Na_2Cu(SO_4)_2$	saranchinaite	atoms	$Na_2Cu(SO_4)_2$	saranchinaite
Cu1−O14	1.929(2) [0.51]	1.947(7) [0.49]	Cu3−O1	1.928(2) [0.51]	1.936(7) [0.50]
Cu1−O19	1.938(2) [0.50]	1.945(7) [0.49]	Cu3−O4	1.938(2) [0.50]	1.946(7) [0.49]
Cu1−O5	2.020(2) [0.40]	2.027(8) [0.39]	Cu3−O7	1.946(2) [0.49]	1.952(7) [0.48]
Cu1−O15	2.025(2) [0.39]	2.041(7) [0.38]	Cu3−O3	1.968(2) [0.46]	1.970(7) [0.46]
Cu1−O23	2.287(2) [0.19]	2.283(8) [0.20]	Cu3−O31	2.352(2) [0.16]	2.352(7) [0.16]
Cu1−O29	2.839(3) [0.04]	2.777(9) [0.05]	Cu3−O9	2.938(2) [0.03]	2.968(7) [0.03]
Cu1−O32	*3.065(3) [0.02]*	*3.100(9) [0.02]*	Cu3−O24	3.012(3) [0.03]	3.030(7) [0.03]
av [BVS]	2.173 [2.03]	2.170 [1.98]	av [BVS]	2.297 [2.17]	2.308 [2.14]
Cu2−O13	1.947(2) [0.48]	1.943(7) [0.49]	Cu4−O30	1.960(2) [0.47]	1.975(7) [0.45]
Cu2−O26	1.950(2) [0.48]	1.954(7) [0.48]	Cu4−O16	1.962(2) [0.47]	1.971(7) [0.46]
Cu2−O3	1.951(2) [0.48]	1.959(7) [0.47]	Cu4−O18	1.979(2) [0.45]	1.985(7) [0.44]
Cu2−O6	1.961(2) [0.47]	1.963(7) [0.47]	Cu4−O12	1.980(2) [0.44]	1.980(7) [0.44]
Cu2−O2	2.264(2) [0.21]	2.264(7) [0.21]	Cu4−O9	2.260(2) [0.21]	2.261(7) [0.21]
Cu2−O23	2.882(2) [0.04]	2.921(8) [0.04]	Cu4−O31	2.942(2) [0.03]	2.950(7) [0.03]
Cu2−O17	2.954(2) [0.03]	2.747(7) [0.04]	*Cu4−O10*	*3.101(2) [0.02]*	*3.089(7) [0.02]*
av [BVS]	2.273 [2.19]	2.250 [2.18]	av [BVS]	2.181 [2.06]	2.187 [2.03]

[a]Interatomic distances with bond valence values <0.03 vu are given in italics.

formation of an unidentified phase, which disappears at around 500 °C. The second endothermic peak observed at 506 °C indicates the total disappearance of synthetic $Na_2Cu(SO_4)_2$ with a formation of $Na_2Cu_3O(SO_4)_3$ composition (synthetic analogue of puninite[40]), which remains stable until ~530 °C. The third endothermic intense peak centered at 535 °C can be associated with the final decomposition of polyanionic $Na_2Cu_3O(SO_4)_3$ into Na_2SO_4, CuO, and unidentified phase(s). Exothermic peaks at 523 and 401 °C found on the reverse DTA curve are related to recrystallization processes.

Optical Properties. The green color of $Na_2Cu(SO_4)_2$ corresponds well to the optical reflection spectrum with an intense maximum in the region of 500−550 nm (Figure 4). The optical band

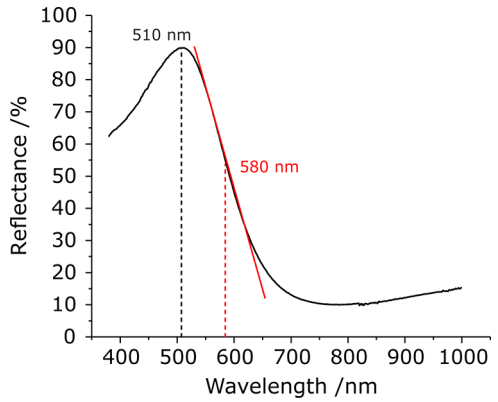

Figure 4. Light reflectivity from $Na_2Cu(SO_4)_2$ powder measured with a PerkinElmer Lambda 1050 spectrophotometer at room temperature.

gap E_g can be estimated as ca. 580 nm. The most powerful peak in the spectrum is precisely the second harmonic radiation at $\lambda_{2\omega}$ = 0.532 μm, which may be excited in a noncentrosymmetric substance under neodymium laser radiation with λ_ω = 1.064 μm. Such an adverse match complicates to some degree a neodymium laser application for determination of the nonlinear optical activity of $Na_2Cu(SO_4)_2$ in the usual transmitted light scheme.[41]

An intense impulse YAG:Nd laser was used as a source of radiation at wavelength λ_ω = 1.064 μm, while second harmonics (SHs) were registered in the reflection mode. The green light of SH generated in the powder sample ($\lambda_{2\omega}$ = 0.532 μm) was selected in the backward scan using colored glass filters. Then the SH signal was registered with a photomultiplier and its intensity $I_{2\omega}$ measured by a lock-in integrator. The measured signal from the sample under investigation was calibrated in relation to a quartz standard. The $Na_2Cu(SO_4)_2$ powder had nearly the same dispersion as an α-quartz powder used as a reference. The value $Q = I_{2\omega}/I_{2\omega}(SiO_2)$ = 0.2 was found to present the SHG activity of $Na_2Cu(SO_4)_2$ on both heating and cooling between room temperature and 400 °C. In order to correct this value for the SH emission in the colored substance, it is necessary to multiply it by a factor of 10 corresponding to the 1/10 share of light at $\lambda_{2\omega}$ = 0.532 μm penetrating through $Na_2Cu(SO_4)_2$ particles. Because nonlinear coefficients of two materials are related to the square roots of Q, we estimate the averaged nonlinear coefficient for $Na_2Cu(SO_4)_2$ to be $\langle d \rangle = 1.4[d_{14}(SiO_2)] \approx 0.5$ pm/V. This is very close to the nonlinearities of earlier investigated sulfates such as $LiKSO_4$ and $Li_2SO_4{\cdot}H_2O$ with nonlinear coefficients d_{33} = 0.71 pm/V and d_{22} = 0.4 pm/V, respectively.[42]

Electrochemical Measurements. Electrochemical tests were performed in Swagelok-type cells assembled in an argon-filled glovebox. Electrodes were prepared by ball milling (15 min) in air of a polycrystalline sample of $Na_2Cu(SO_4)_2$ with carbon C_{sp} as a conductive additive (83.3:16.7 wt %). About 8 mg of the as-prepared composite was studied as a cathode separated from either Na or Li metal as a negative electrode by two sheets of Whatman GF/D borosilicate glass fiber soaked in a liquid electrolyte. Solutions of $NaPF_6$ or $LiPF_6$ (1 M) in EC:DMC (1:1 weight ratio) were used as the electrolytes. Fluoroethylene carbonate (FEC; 3% mass) was added to the Na-based electrolyte. Galvanostatic tests were conducted with an Apple Mac Pile II potentiostat.

Magnetic Measurements. The magnetic characterization of synthetic $Na_2Cu(SO_4)_2$ was performed on a polycrystalline sample using a MPMS SQUID-VSM (Quantum Design) magnetometer in temperature and field ranges of 1.8−400 K and 0−7 T, respectively. The temperature dependence of the magnetization was determined under various magnetic fields after cooling the sample in a field (FC, field cooling) or in a zero field (ZFC, zero-field cooling).

RESULTS AND DISCUSSION

Structure Analysis. $Na_2Cu(SO_4)_2$ crystallizes in the noncentrosymmetric monoclinic space group $P2_1$. The structural data for the synthetic phase are in good agreement with the data reported for natural saranchinaite containing in addition a small amount of potassium.[28] Nevertheless, one interesting point is worth a special discussion.

The unusual structural feature of its crystal structure is an atypical coordination environment of O around Cu^{2+} sites. In the structure, there are four crystallographically independent Cu positions. Each Cu site forms four short Cu−O_{eq} bonds in its equatorial plane that define regular CuO_4 squares (average $\langle Cu{-}O_{eq} \rangle$ = 1.978, 1.952, 1.945, and 1.970 Å for Cu1, Cu2, Cu3, and Cu4, respectively). Each square is complemented by one longer apical Cu−O_{ap} bond, thus forming rather regular CuO_5 tetragonal pyramids ($\langle Cu{-}O_{ap} \rangle$ = 2.287, 2.264, 2.352, and 2.260 Å for Cu1, Cu2, Cu3, and Cu4, respectively) typical for copper oxide compounds.

All Cu^{2+} cations also have additional weaker and longer (2.8−3.1 Å) contacts with two O_{add} atoms each. Bond valence calculations for Cu−O_{add} bonds dictate that they should be taken into consideration and included in the coordination sphere of Cu^{2+} cations. A Cu−O distance of ~3.03 Å provides 0.03 vu and contributes about 1.5% to the overall bond valence sum (BVS). Therefore, Cu−O distances with bond valence ≥0.03 vu were considered (see Table 2). Accordingly, the coordination spheres of the Cu1 and Cu4 sites can be described as distorted octahedra with one additional sixth O ligand each (Cu−O_{sixth} = 2.839 Å (0.04 vu) and 2.942 Å (0.03 vu) for Cu1 and Cu4, respectively), which is common for minerals and synthetic compounds.[43] The most remarkable observation concerns the coordination of the Cu2 and Cu3 sites adopting scarce heptahedral CuO_7 coordination (Figure 5) with two additional oxygen atoms O located at distances of 2.882 Å (0.04 vu), 2.954 Å (0.03 vu) and 2.938 Å (0.03 vu), 3.012 Å (0.03 vu) from Cu2 and Cu3 centers, respectively.

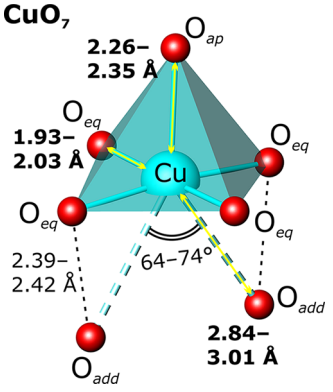

Figure 5. Heptahedral coordination of Cu^{2+} in the structure of $Na_2Cu(SO_4)_2$.

Each pair of these additional O anions is located geometrically strictly below two O corners of one the diagonals of square bases of the CuO_5 pyramids with $O_{eq}\cdots O_{add}$ distances of 2.39–2.42 Å for the Cu1–Cu4 sites. The $O_{add}–Cu–O_{add}$ angles are in the range between 64 and 74°. This unusual relatively regular 7-fold coordination of Cu^{2+} is very rare for inorganic compounds under ambient conditions.[28,44,45] The coordination of Cu^{2+} sites in the crystal structure of $Na_2Cu(SO_4)_2$ is shown in Figure S2.

The atomic environment of eight Na^+ cations in the structure of synthetic $Na_2Cu(SO_4)_2$ does not change significantly from those reported for saranchinaite (Table S3). Note that the only differences in the coordination of the Na5 site in both structures (Figure 6) are caused by the partial substitution of Na^+ by K^+ in the structure of the mineral phase.

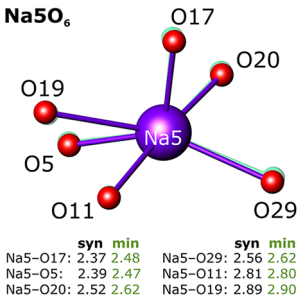

Figure 6. Geometrical environment of the Na5 site in the structure of synthetic $Na_2Cu(SO_4)_2$. Projections of the O positions in the structure of saranchinaite are shown in green for comparison. Distances are given in Å.

In the crystal structure of $Na_2Cu(SO_4)_2$, all copper polyhedra are connected to each other via medium/long Cu- -O_{add}- - -Cu bridges and polymerized into polar chains running along the *c* direction as shown in Figure 7. Thus, the noncentrosymmetric symmetry of the structure is justified by the "up" only orientation of CuO_5 pyramids along [001]. Note that Cu2 and Cu3 metal centers are located relatively close to each other (Cu2···Cu3 = 3.36 Å; cf. Cu3···Cu4 = 4.90 Å) and share a common O corner of their square O bases, forming a dimer. Such a close arrangement of the two neighboring Cu2 and Cu3 polyhedra may be responsible for overall slight shortening of the Cu–O contacts, thus favoring unusual heptahedral $Cu2O_7$ and $Cu3O_7$ coordination polyhedra. Indeed, the average Cu–O distances to the seven closest O ligands for Cu2 (2.273 Å) and Cu3 (2.297 Å) are slightly smaller than those for Cu1 (2.300 Å) and Cu4 (2.312 Å). The terminal oxygen atoms of every copper polyhedron are bridged by sulfate SO_4 anions to form a complex 3D framework with a large system of pores and cavities filled by Na^+ cations (Figure 8c).

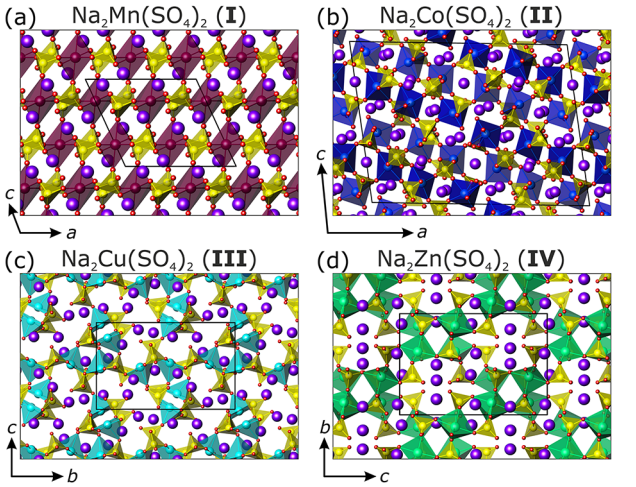

Figure 8. Projections of the crystal structures of $Na_2M(SO_4)_2$: *M* = Mn (a), structure type **I**; Co (b), structure type **II**; Cu (c), structure type **III**; Zn (d), structure type **IV**. Sulfate, manganese, cobalt, copper, and zinc polyhedra are shown in yellow, plum, blue, cyan, and green, respectively; sodium is denoted by purple balls.

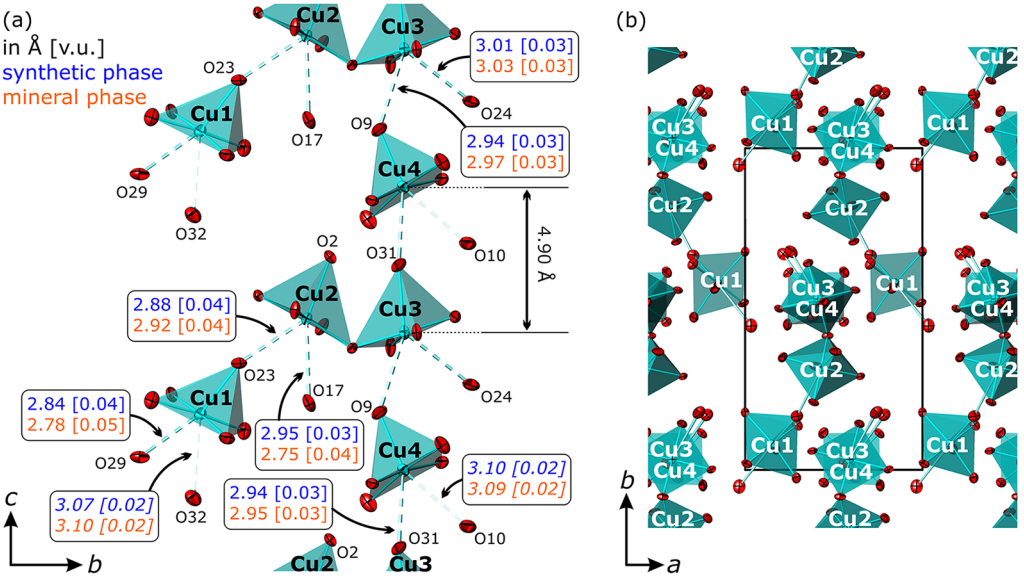

Figure 7. Interconnection of CuO_5 pyramids and comparison of bond lengths and valence values for long Cu–O distances in the structures of synthetic (blue) and mineral (orange) phases. Cu–O contacts <0.03 vu are given in italics. Displacement ellipsoids are drawn at the 80% probability level.

Table 3. Crystallographic Data and Preparation Methods of Anhydrous $Na_2M(SO_4)_2$ Phases (M^{2+} = Transition Metal)

formula	struct type ($I_{G,total}$)	a, b, c (Å); β (deg); (V (Å^3)); space group	preparation method	ref
$Na_2Mn(SO_4)_2$	I (72.211)	10.101, 8.240, 8.730; 114.6 (660.5); $C2/c$	in situ XRD at 227 °C from $Na_2Mn_{1.17}(SO_4)_2S_{0.33}O_{1.17}(H_2O)_2$	78
$Na_2Co(SO_4)_2$	II (828.523)	23.346, 10.300, 17.412; 98.9 (4137.0); $C2/c$	solid-state synthesis via an equimolar reaction of $CoSO_4 \cdot 7H_2O$ and Na_2SO_4 at 550 °C in Ar	21, 79
$Na_2Ni(SO_4)_2$	II (828.523)	23.225, 10.262, 17.335; 99.0 (4080.2); $C2/c$	solid-state synthesis via an equimolar reaction of Na_2SO_4 and $NiSO_4 \cdot 6H_2O$ at 550 °C in Ar	22, 79
$Na_2Cu(SO_4)_2$	III (592.846)	8.971, 15.548, 10.142; 107.2 (1351.7); $P2_1$	(a) evaporation from an aqueous solution containing nearly equimolar quantities of Na_2SO_4 and $CuSO_4 \cdot 5H_2O$	a
			(b) slow cooling of the melt containing equimolar quantities of $CuSO_4$ and Na_2SO_4 in an evacuated ampule from 950 °C	
$Na_2Zn(SO_4)_2$	IV (496.846)	8.648, 10.323, 15.103; 90.9 (1348.1); $P2/n$	slow cooling of the melt containing equimolar quantities of ZnO and $Na_2S_2O_7$ in an evacuated ampule from 500 °C	80
α-$Na_2Cd(SO_4)_2$	I (72.211)	10.059, 8.225, 8.656; 114.6 (651.0); $C2/c$	evaporation from an aqueous solution containing equimolar quantities of $CdSO_4$ and Na_2SO_4	23, 81, 82
β-$Na_2Cd(SO_4)_2$	V (no str. data)	15.114, 9.051, 12.779; 126.5 (1405.7); $P2_1/c$	fast quenching of the α-$Na_2Cd(SO_4)_2$-based melt from 570 °C	23

[a]This work.

Table 4. Hydrated $Na_2M(SO_4)_2(H_2O)_x$ (M = Transition Metal; x = 2, 4, 6) Compounds: Reported Results of Phase Transformations upon Heating, Average M−O Bond Lengths, and Distortion Δ_d

formula/⟨M−O⟩ (Å); $10^4\Delta_d$	ref	$r_{ion}(M^{2+})$ (Å)	formula (struct type)/⟨M−O⟩ (Å); $10^4\Delta_d$	transition temp (°C)	ref
			Kröhnkite Type		
$Na_2Mn(SO_4)_2(H_2O)_2$/2.152; 3	24, 58, 61, 83, 84	0.83	→$Na_{2+\delta}Mn_{2-\delta/2}(SO_4)_3$/2.221; 3	200	24
$Na_2Fe(SO_4)_2(H_2O)_2$/2.125; 11	17−20	0.78	→$Na_{2+\delta}Mn_{2-\delta/2}(SO_4)_3$/2.148; 10 + $Na_6Fe(SO_4)_4$	300	17, 24
$Na_2Co(SO_4)_2(H_2O)_2$/2.141; 4	58, 61	0.75	→$Na_2Co(SO_4)_2$ (II)/2.109; 37[a]	190	61
$Na_2Cu(SO_4)_2(H_2O)_2$/2.138; 11	28, 58, 85−87	0.73	→$Na_2Cu(SO_4)_2$ (III)/2.173; 257[a]	200	28
$Na_2Cd(SO_4)_2(H_2O)_2$/2.287; 2	23, 83, 84	0.95	→α-$Na_2Cd(SO_4)_2$ (I)/2.317; 7	550	23
			Fairfieldite Type		
$Na_2Ni(SO_4)_2(H_2O)_2$/2.037; 6	58, 61	0.69	→$Na_2Ni(SO_4)_2$ (II)/2.077; 14[a]	240	61
			Blödite Type		
$Na_2Fe(SO_4)_2(H_2O)_4$/2.129; 2	17, 21, 88	0.78	→$Na_2Fe(SO_4)_2$ (II)/no struct data	120	21
$Na_2Co(SO_4)_2(H_2O)_4$/2.101; 2	21, 89, 90	0.75	→$Na_2Co(SO_4)_2$ (II)/2.109; 37[a]	180	21
$Na_2Ni(SO_4)_2(H_2O)_4$/2.065; 1	22, 89, 91	0.69	→$Na_2Ni(SO_4)_2$ (II)/2.077; 14[a]	140	22
$Na_2Zn(SO_4)_2(H_2O)_4$/2.101; 2	89, 92−94	0.74	→loss of water/no struct data	138	94
$Na_2Cd(SO_4)_2(H_2O)_4$/2.276; 2	23	0.95	no information		
			Picromerite Type		
$Na_2Co(SO_4)_2(H_2O)_6$/2.092; 2	95	0.75	→loss of water/no struct data	101	95
$Na_2Ni(SO_4)_2(H_2O)_6$/2.056; 1	96	0.69	→loss of water/no struct data	110	96
$Na_2Cu(SO_4)_2(H_2O)_6$/2.090; 20	97	0.73	no information		

[a]Average values for several M^{2+} sites in the given structure.

Crystal Growth of Anhydrous Na-Containing Sulfates. The synthesis of anhydrous sulfates is quite a challenging task. In most cases, the sulfates demonstrate a relatively low thermal stability accompanied by decomposition of sulfate groups to SO_3 and $SO_2 + O_2$.[46] As a consequence, an inert atmosphere or lower than atmospheric pressure (vacuum) is used to maintain the stability of sulfate anions during the chemical reaction. For example, alluaudite-type $Na_{2.32}Co_{1.84}(SO_4)_3$[47] and $Na_{2.5}Fe_{1.75}(SO_4)_3$[48] compounds were synthesized in Ar/N_2-regulated furnaces by low-temperature solid-state reactions at 350 °C. Crystal growth from a melt in the temperature range of 460−500 °C in an artificial inert-flow reactor was used for the preparation of V-containing sodium sulfates $NaV(SO_4)_2$,[49] $Na_3V(SO_4)_3$,[50] $Na_8(VO)_2(SO_4)_6$,[51] and $Na_2VO(SO_4)_2$.[52] Similar experiments carried out in sealed Ag containers or quartz ampules led to crystallization of $Na_5(CuO_2)(SO_4)$[53] and $Na_{11}(CuO_4)(SO_4)_3$[54] or of $Na_8(CoO_3)(SO_4)_2$[55] and $Na_4(MoO_2)(SO_4)_3$,[56] respectively. The experimental details of synthesis methods of the compounds in the $Na_2M(SO_4)_2$ (M = Mn, Co, Ni, Cu, Zn, Cd) family are summarized in Table 3 for the reader's convenience.

Among the others, it is noteworthy that anhydrous $Na_{2.74}Mn_{1.86}(SO_4)_3$,[24] $Na_{2.76}Mn_{1.78}(SO_4)_3$,[24] and $Na_3Fe(SO_4)_3$[57] were prepared by a dehydration of mineral-type hydrated phases: from the kröhnkite-type $Na_2Mn(SO_4)_2(H_2O)_2$ and sideronatrite-type $Na_2Fe(SO_4)_2(OH)(H_2O)_3$ compounds, respectively. Moreover, the synthetic $Na_2Cu(SO_4)_2$ compound reported in this work can be also produced from the kröhnkite mineral itself by a dehydration process, as described in the Experimental Section. Remarkably, dehydration processes of the hydrated phases with similar chemical formulas may lead to different structural architectures, as will be discussed below. These observations in agreement with similar ideas already reported[23,24] suggest that abundant hydrated sulfate minerals may be considered as low-cost prospective precursors for the design of novel anhydrous compounds with various structure types.

Dehydration of the $Na_2M(SO_4)_2(H_2O)_x$ Compositions. In the present work we focus on several families of mineral-like

groups of hydrated $Na_2M(SO_4)_2(H_2O)_x$ transition-metal sulfates: namely, the picromerite (x = 6, M = Co, Ni, Cu) group, the blödite (x = 4, M = Fe, Co, Ni, Zn, Cd) group, the kröhnkite (x = 2, M = Mn, Fe, Co, Cu, Cd) group, and the only known phase isostructural with fairfieldite (x = 2, M = Ni). A key structural difference between the monoclinic kröhnkite-type and triclinic fairfieldite-type structures is the different hydrogen-bonding network that links the chains of $M(SO_4)_4(H_2O)_2$ composition.[58] All of the phases belonging to these groups are summarized in Table 4. It is of interest to note that the analysis of the reported phase transitions of these phases upon dehydrating reveals intriguing peculiarities. In most cases, the loss of water molecules led to the formation of $Na_2M(SO_4)_2$ anhydrous compositions. However, note that the phase transitions for the isostructural kröhnkite-type (x = 2) compounds resulted in a formation of the anhydrous sulfates of different structure types (Table 4). The observed variations of the structural transformations cannot be explained by ionic (high spin) mismatch between the size of transition metals (Cd > Mn > Fe > Co > Zn > Cu > Ni)[59] only but implies a subtle interplay between several factors simultaneously.

From a structural point of view, the H_2O molecules in the structures of these hydrates can be regarded as a "glue"[60] binding the other structural units. Thus, the release of water upon dehydration may lead to a structural transformation in accordance with the different preferred stereochemical coordination of metal cations as well. That is, for example, the $Na_2Cu(SO_4)_2(H_2O)_2$ phase transforms to anhydrous $Na_2Cu(SO_4)_2$[28] with a well-pronounced Jahn–Teller distortion for Cu^{2+} in its structure, whereas the structure of $Na_2Mn(SO_4)_2(H_2O)_2$ transforms to the alluaudite-type $Na_{2+\delta}Mn_{2-\delta/2}(SO_4)_3$ phase.[24] In the latter case, we suggest that the difference in transition-metal ionic radii (Mn^{2+} (0.83 Å) > Cu^{2+} (0.73 Å)) is a crucial factor for the structural transformation. Indeed, a similar kröhnkite → alluaudite transformation has been observed for the dehydration of $Na_2Fe(SO_4)_2(H_2O)_2$ with a relatively large Fe^{2+} cationic radius (0.78 Å).[17,24] In contrast, the Co- and Ni-containing $Na_2M(SO_4)_2(H_2O)_2$ compositions with a smaller size of cations (0.75 and 0.69 Å, respectively) transform to another structural type of anhydrous $Na_2M(SO_4)_2$ exhibiting no pronounced distortion effects for transition-metal cations.[61]

In order to get a deeper insight into the dehydration effects on the crystal structures, the coordinations of M^{2+} cations in the structures of the compounds under consideration have been analyzed. In most of the structures, transition-metal cations exhibit octahedral environments of different degrees of distortions except for the $Na_2Cu(SO_4)_2$ phase discussed in the present work. To quantify the degree of distortions of MO_6 polyhedra, the Δ_d parameter defined previously for perovskites,[62] mixed MO_6 (M = Cu, Zn) octahedra in Cu, Zn oxysalt minerals[63] and recently the mixed MnO_nCl_m octahedral coordination environments[64] was used. This parameter concerns the deviation of M–O distances with respect to its average value for each polyhedron and can be calculated as follows: $\Delta_d = (1/6)\sum_{n=1,6}[(d_n - \langle d\rangle)/\langle d\rangle]^2$, where $\langle d\rangle$ is the average M–O distance in a given octahedron (Table 4).

Several observations for the reported phase transformations upon dehydration can be made. The average octahedral M–O distances are increasing upon $Na_2M(SO_4)_2(H_2O)_x$ → $Na_2M(SO_4)_2$ dehydration in most of the structures with the greatest distance difference revealed for the $Na_2Mn(SO_4)_2(H_2O)_2$ → $Na_{2+\delta}Mn_{2-\delta/2}(SO_4)_3$ transformation: from 2.152 to 2.221 Å. The only exception is the $Na_2Co(SO_4)_2(H_2O)_2$ → $Na_2Co(SO_4)_2$ transformation, which results in a shortening of the ⟨Co–O⟩ distance from 2.141 to 2.109 Å. Although these variations of average bond lengths cannot be explained by a simple ionic mismatch, the calculated Δ_d parameter of octahedral distortions can provide more useful information. For the hydrated compositions $Na_2M(SO_4)_2(H_2O)_2$ (M = Cd^{2+}, Mn^{2+}, Fe^{2+}) with octahedra centered by transition metals with larger ionic radii, the octahedral coordination environments are quite regular before ($10^4\Delta_d$ = 2, 3, 11, respectively) as well as after ($10^4\Delta_d$ = 7, 3, 10, respectively) dehydration. In contrast, the degree of octahedral distortions is increasing after transformations for the phases containing the smaller Co^{2+}, Cu^{2+}, and Ni^{2+} cations: from $10^4\Delta_d$ = 4, 11, 6, respectively, for hydrated $Na_2M(SO_4)_2(H_2O)_2$ (M = Co^{2+}, Cu^{2+}, Ni^{2+}) compounds up to $10^4\Delta_d$ = 37, 257, 14, respectively, for anhydrous $Na_2M(SO_4)_2$ (M = Co^{2+}, Cu^{2+}, Ni^{2+}) phases. Note that this strong deviation of the geometrical shape of copper polyhedra from the ideal octahedron in the structure of $Na_2Cu(SO_4)_2$ results from a well-pronounced Jahn–Teller distortion and also suggests considering the coordination of Cu^{2+} in the structure to be distinct from an octahedron.

Structure Types and Structural Complexity of the $Na_2M(SO_4)_2$ Compounds. Since the structural relationships between the crystal structures of hydrates and anhydrous salts have been very recently discussed,[22] it is also of interest to compare different structure types corresponding to various chemical $Na_2M(SO_4)_2$ (M = Mn, Co, Ni, Cu, Zn, Cd) compositions (Table 3). There are five different structure types. Four of them are presented in Figure 8 (the structure type **V** has been reported for metastable β-$Na_2Cd(SO_4)_2$ which was reported without any structural data except for its unit cell parameters[23]).

Two compounds with the largest metal ionic radii (Cd^{2+} = 0.95 Å; Mn^{2+} = 0.83 Å) crystallize in the same structure type denoted herein as **I** (Figure 8a). Here, the transition-metal cations form rather regular octahedra with an average ⟨Cd–O⟩ and ⟨Mn–O⟩ bond lengths of 2.317 and 2.301 Å, respectively.

Despite differences in size (Co (0.75 Å) > Ni (0.69 Å)), the phases containing chemically similar Co^{2+} and Ni^{2+} metals belong to the same structure type **II** (Figure 8b) with quite regular octahedra of transition metals (⟨M–O⟩ = 2.094 and 2.077 Å for M = Co^{2+}, Ni^{2+}, respectively).

We did not find reported structural data for the Fe-containing (Fe^{2+} = 0.78 Å) compound in the literature. Note, however, that Reynaud et al. though succeeded in preparing the iron-based polycrystalline sample with impurities, which also suggests the structure type **II** for $Na_2Fe(SO_4)_2$.[21]

Interestingly, in spite of the observed similarities in unit cell dimensions of the crystal structures of $Na_2Cu(SO_4)_2$ and $Na_2Zn(SO_4)_2$ containing nearly isometric Cu^{2+} (0.73 Å) and Zn^{2+} (0.74 Å) cations, respectively, these structures differ significantly from each other (Figure 8c,d). Again, this may be explained by different preferred coordinations of transition-metal cations. Copper cations have pronounced Jahn–Teller distorted coordination in synthetic $Na_2Cu(SO_4)_2$, which is not typical for Zn^{2+} usually exhibiting[63] a more regular surrounding of ligands in comparison to Cu^{2+}. Indeed, the only two Zn sites in the structure of $Na_2Zn(SO_4)_2$ form relatively regular 5-fold trigonal bipyramids (⟨Zn–O⟩ = 2.043 Å).

It is of interest also to compare polymorphic variations in the $Na_2M(SO_4)_2$ group from the viewpoint of structural

complexity, which can be estimated as a Shannon information content per unit cell ($I_{G,total}$, bits/unit cell (uc)) according to a recently developed approach.[65−67] The $I_{G,total}$ values calculated by using the ToposPro[68] software are given in Table 3. The obtained results show a correlation among the unit-cell volumes, revealing that the structures with large cells of isotypic $Na_2Co(SO_4)_2$ and $Na_2Ni(SO_4)_2$ are the most complex in comparison with the others.

Our results also revealed that the structure of $Na_2Cu(SO_4)_2$ ($I_{G,total}$ = 592.846 bits/uc) is more complex than that of $Na_2Zn(SO_4)_2$ ($I_{G,total}$ = 496.846 bits/uc) with close unit cell dimensions and both crystallizing in the monoclinic crystal system. This observation is consistent with the general expectation that the absence of an inversion center and a pronounced Jahn−Teller distortion in the structure of $Na_2Cu(SO_4)_2$ may lead to an increase in structural complexity. The estimated $I_{G,total}$ values allow classification of the structure types **I** and **II**−**IV** as *simple* and *complex*, respectively. *Simple* and *complex* structures are 34% and 0.03% of all reported inorganic compounds.[69]

Electrochemistry. The Cu^{2+}/Cu^{3+} redox potential has been predicted to provide a high operating voltage in rechargeable battery systems.[70] However, this phenomenon still lacks further studies and an overall understanding. For example, a recent report revealed a very limited electrochemical performance for $K_2Cu_2(SO_4)_3$ and $K_2Cu_3O(SO_4)_3$.[71] Nevertheless, it has been also demonstrated that $Li_2Cu_2O(SO_4)_2$ is able to offer a reversible electrochemical activity at 4.7 V vs Li^+/Li corresponding to the $Cu^{2+/3+}$ redox transition associated with the reversible change of 0.3 Li.[70] Hence, as a further attempt to explore the oxidation of Cu^{2+} to Cu^{3+} in the course of an electrochemical reaction, several tests were performed using $Na_2Cu(SO_4)_2$ as a cathode material, providing a theoretical capacity of ∼89 mAh/g (for 1 e^- transfer per Cu cation).

The electrochemical behavior of $Na_2Cu(SO_4)_2$ either vs Na or vs Li was examined using Swagelok-type cells assembled in an argon-filled glovebox and cycled at room temperature. Unfortunately, difficulties in Na^+ extraction have been encountered during the electrochemical cycling in Na- and Li-based types of the cells, and the removal of a significant amount of Na^+ from the structure of $Na_2Cu(SO_4)_2$ failed. As seen from Figure S3a, the irreversible extraction is limited to a value of only 0.04 Na^+ per formula unit at ∼4.0 V vs Li^+/Li. The cycling of the $Na_2Cu(SO_4)_2$-based cathode vs Na reveals the occurrence of a probable redox process at a higher voltage of around 4.7 vs Na^+/Na (Figure S3b), which is beyond the voltage stability window of the electrolytes available up to now. Thus, $Na_2Cu(SO_4)_2$ is not suitable as a cathode material.

The bond valence energy landscape (BVEL) defined using the BondStr software (FullProf suite[72]) also demonstrates that there are no interconnected pathways for sodium migration in the structure of $Na_2Cu(SO_4)_2$ (Figure 9) considering a percolation energy of 1.6 eV reported for the movement of Na^+ in polyanionic compounds.[73,74]

Magnetism. The magnetic properties of $Na_2Cu(SO_4)_2$ reflect well its crystal structure in the sense that, according to the orientation of the $d_{x^2-y^2}$ magnetic orbitals (Cu^{2+}, d^9, S = 1/2) roughly assigned to the CuO_4 square planes, no magnetic overlap is achieved apart from the dimers formed by Cu2 and Cu3. Here, the Cu2−O3−Cu3 angle is 118.3°, which suggests significant superexchange contribution. Accordingly, we considered half of copper atoms as mainly paramagnetic and

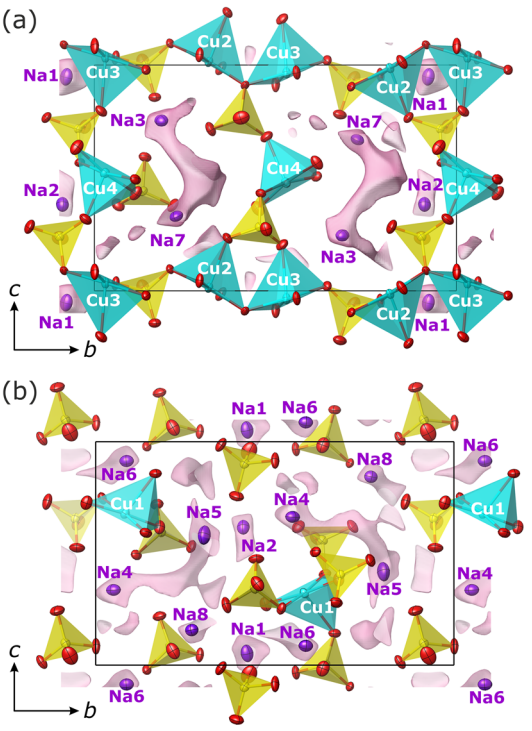

Figure 9. Two cross sections at 1/2 translation along the *a* axis demonstrating sodium diffusion pathways shown in pink inside the structure of $Na_2Cu(SO_4)_2$ defined from BVEL with a percolation energy of 1.6 eV. Displacement ellipsoids are drawn at the 80% probability level.

the other half as strongly engaged in antiferromagnetic dimer interactions. The Curie−Weiss fit shown in Figure 10a gives μ_{eff} = 1.85 μ_B/Cu and Θ_{CW} = −17.2 K, which validate

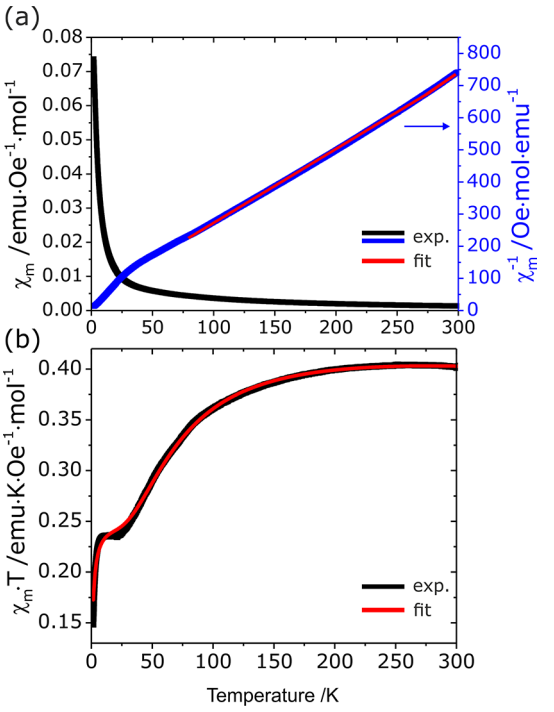

Figure 10. Thermal evolution of the magnetic susceptibility (a) and temperature dependence of χ_T (b) for $Na_2Cu(SO_4)_2$.

predominant antiferromagnetic exchanges. The accident observed below ca. 50 K mainly occurred due to the intradimer interactions, as detailed below. It was fitted using an $\chi_T(T)$ plot (Figure 10b) through the susceptibility equation

$$\chi_{Cu} = \rho\frac{Ng^2\beta^2}{kT(3 + e^{-J/kT})} + (1 - \rho)\frac{Ng^2\beta^2}{4k(T - \Theta)} + \chi_{dia}$$

where the first term represents the intradimer susceptibility of the Cu fraction ρ following the Bleaney–Bowers equation,[75] while the second term is the complementary Cu^{2+} paramagnetism with interaction quantified by Θ, N, g, β, k, and χ_{dia} having their usual meanings.

The fit was first constrained to ρ = 50% but then greatly improved on relaxing g = 2.237(3), J/k = 138.7(7) K (96.4 cm^{-1}), Θ = −0.95(1) K, $\chi_{dia} = -21 \times 10^{-6}$ emu/mol, and ρ = 45.8(2)%. The g value is in good agreement with the effective moment greater than the "spin-only" value (μ_{eff} = 1.74 μ_B), while Θ and J/k confirm a strong AFM dimer in a nearly paramagnetic matrix. The ratio ρ suggests a few percent of extra intrinsic and/or extrinsic paramagnetic impurities, not revealed by XRD.

CONCLUSION

The novel anhydrous sulfate $Na_2Cu(SO_4)_2$ has been synthesized by two different methods for the first time and structurally characterized. A unusual structural feature of the new synthetic $Na_2Cu(SO_4)_2$ phase is the presence of heptahedral CuO_7 polyhedra with two additional long and weak Cu–O distances, which are interconnected through common O corners in polar chains.

Electrochemical, magnetic, thermal, and optical behaviors of $Na_2Cu(SO_4)_2$ have been also determined. The title compound demonstrates a very limited electrochemical activity and highly stable Na sublattice (that is, low mobility of Na ions) in its crystal structure. The magnetic behavior of $Na_2Cu(SO_4)_2$ reflects its crystal structure with half of the copper cations as mainly paramagnetic and the other half as strongly engaged in antiferromagnetic dimer interactions.

Analysis of the synthesis methods reported for the preparation of other Na-containing anhydrous sulfates and our studies of the structural polymorphism in the group of $Na_2M(SO_4)_2$ (M = Mn, Co, Ni, Cu, Zn, Cd) compositions suggest that abundant hydrated sulfate minerals may be considered as low-cost prospective precursors for the design of novel compounds of various structure types.

We believe that the preparation of synthetic analogues of known minerals is able to serve fundamental science well.[76] It can help to solve complex crystal structures (e.g., synthetic nyerereite[25]) or to make a model system for an investigation of various physical properties in the laboratory, when it is difficult to obtain samples with a good crystallinity and sufficient amount in nature (e.g., zeolites[77]). Hence, minerals and mineral-like synthetic compounds can serve as sources of inspiration for elaboration of new materials in many research areas the solid-state chemistry.

ASSOCIATED CONTENT

Supporting Information

The Supporting Information is available free of charge on the ACS Publications website at DOI: 10.1021/acs.cgd.8b01658.

Fractional atomic coordinates, atomic displacement parameters, Na–O bond lengths in the structures of new $Na_2Cu(SO_4)_2$ and saranchinaite, selected HTPXRD patterns revealing phase transformations of saranchinaite with increasing temperature, coordination of Cu^{2+} in the structure of synthetic $Na_2Cu(SO_4)_2$, and electrochemical curves (PDF)

Accession Codes

CCDC 1866049 contains the supplementary crystallographic data for this paper. These data can be obtained free of charge via www.ccdc.cam.ac.uk/data_request/cif, or by emailing data_request@ccdc.cam.ac.uk, or by contacting The Cambridge Crystallographic Data Centre, 12 Union Road, Cambridge CB2 1EZ, UK; fax: +44 1223 336033.

AUTHOR INFORMATION

Corresponding Authors

*E-mail for V.M.K.: kovrugin_vm@hotmail.com.
*E-mail for O.I.S.: o.siidra@spbu.ru.

ORCID

Vadim M. Kovrugin: 0000-0002-9010-625X
Oleg I. Siidra: 0000-0003-1908-3152
Olivier Mentré: 0000-0002-1822-6003
Christian Masquelier: 0000-0001-7289-1015

Notes

The authors declare no competing financial interest.

ACKNOWLEDGMENTS

This work was financially supported by the Russian Science Foundation through grant 16-17-10085. V.M.K. was supported by the NAIADES project of the Regional Council of Picardie and the University of Picardie Jules Verne. The Ph.D. thesis of D.O.N. was carried out within the framework of the international French–Russian cotutorial Ph.D. program (CampusFrance). The Fonds Européen de Développement Régional (FEDER), the CNRS, the Région Nord Pas-de-Calais, and the Ministère de l'Education Nationale de l'Enseignement Supérieur et de la Recherche are acknowledged for funding the X-ray diffractometers. D.O.N. also acknowledges support of the Saint-Petersburg State University through its internal travel grant 3.42.713.2017 for a visit to the LRCS. The authors also acknowledge Nora Djelal and Jean-Luc Paugam for their technical assistance with the DTA and IR analyses. We also thank an anonymous reviewer for constructive comments and useful suggestions.

REFERENCES

(1) Krivovichev, S. V. In *Minerals as Advanced Materials II*; Krivovichev, S. V., Ed.; Springer Berlin Heidelberg: Berlin, Heidelberg, 2012.

(2) Depmeier, W. Minerals as Advanced Materials. *Cryst. Res. Technol.* **2009**, *44*, 1122–1130.

(3) McMillen, C. D.; Kolis, J. W. Hydrothermal Synthesis as a Route to Mineralogically-Inspired Structures. *Dalt. Trans.* **2016**, *45*, 2772–2784.

(4) Ackiss, S. E.; Wray, J. J. Occurrences of Possible Hydrated Sulfates in the Southern High Latitudes of Mars. *Icarus* **2014**, *243*, 311–324.

(5) Karunatillake, S.; Wray, J. J.; Gasnault, O.; McLennan, S. M.; Deanne Rogers, A.; Squyres, S. W.; Boynton, W. V.; Skok, J. R.; Button, N. E.; Ojha, L. The Association of Hydrogen with Sulfur on Mars across Latitudes, Longitudes, and Compositional Extremes. *J. Geophys. Res. E Planets* **2016**, *121*, 1321–1341.

(6) Barpanda, P. Sulfate Chemistry for High-Voltage Insertion Materials: Synthetic, Structural and Electrochemical Insights. *Isr. J. Chem.* **2015**, *55*, 537−557.
(7) Rousse, G.; Tarascon, J. M. Sulfate-Based Polyanionic Compounds for Li-Ion Batteries: Synthesis, Crystal Chemistry, and Electrochemistry Aspects. *Chem. Mater.* **2014**, *26*, 394−406.
(8) Lu, J.; Nishimura, S.; Yamada, A. Polyanionic Solid-Solution Cathodes for Rechargeable Batteries. *Chem. Mater.* **2017**, *29*, 3597−3602.
(9) Shiva, K.; Singh, P.; Zhou, W.; Goodenough, J. B. $NaFe_2PO_4(SO_4)_2$: A Potential Cathode for a Na-Ion Battery. *Energy Environ. Sci.* **2016**, *9*, 3103−3106.
(10) Masquelier, C.; Croguennec, L. Polyanionic (Phosphates, Silicates, Sulfates) Frameworks as Electrode Materials for Rechargeable Li (or Na) Batteries. *Chem. Rev.* **2013**, *113*, 6552−6591.
(11) Lander, L.; Tarascon, J.-M.; Yamada, A. Sulfate-Based Cathode Materials for Li- and Na-Ion Batteries. *Chem. Rec.* **2018**, *18*, 1394−1408.
(12) Padhi, A. K.; Nanjundaswamy, K. S.; Masquelier, C.; Goodenough, J. B. Mapping of Transition Metal Redox Energies in Phosphates with NASICON Structure by Lithium Intercalation. *J. Electrochem. Soc.* **1997**, *144*, 2581−2586.
(13) Singh, P.; Shiva, K.; Celio, H.; Goodenough, J. B. Eldfellite, $NaFe(SO_4)_2$: An Intercalation Cathode Host for Low-Cost Na-Ion Batteries. *Energy Environ. Sci.* **2015**, *8*, 3000−3005.
(14) Yu, C.-J.; Choe, S.-H.; Ri, G.-C.; Kim, S.-C.; Ryo, H.-S.; Kim, Y.-J. Ionic Diffusion and Electronic Transport in Eldfellite $Na_xFe(SO_4)_2$. *Phys. Rev. Appl.* **2017**, *8*, 024029.
(15) Ri, G.-C.; Choe, S.-H.; Yu, C.-J. First-Principles Study of Mixed Eldfellite Compounds $Na_x(Fe_{1/2}M_{1/2})(SO_4)_2$ ($x = 0-2$, M = Mn, Co, Ni): A New Family of High Electrode Potential Cathodes for the Sodium-Ion Battery. *J. Power Sources* **2018**, *378*, 375−382.
(16) Banerjee, A.; Araujo, R. B.; Ahuja, R. Unveiling the Thermodynamic and Kinetic Properties of $Na_xFe(SO_4)_2$ ($x = 0-2$): Toward a High-Capacity and Low-Cost Cathode Material. *J. Mater. Chem. A* **2016**, *4*, 17960−17969.
(17) Barpanda, P.; Oyama, G.; Ling, C. D.; Yamada, A. Kröhnkite-Type $Na_2Fe(SO_4)_2{\cdot}2H_2O$ as a Novel 3.25 V Insertion Compound for Na-Ion Batteries. *Chem. Mater.* **2014**, *26*, 1297−1299.
(18) Meng, Y.; Zhang, S.; Deng, C. Superior Sodium−lithium Intercalation and Depressed Moisture Sensitivity of a Hierarchical Sandwich-Type Nanostructure for a Graphene−sulfate Composite: A Case Study on $Na_2Fe(SO_4)_2{\cdot}2H_2O$. *J. Mater. Chem. A* **2015**, *3*, 4484−4492.
(19) Meng, Y.; Li, Q.; Yu, T.; Zhang, S.; Deng, C. Architecture−property Relationships of Zero-, One- and Two-Dimensional Carbon Matrix Incorporated $Na_2Fe(SO_4)_2{\cdot}2H_2O$/C. *CrystEngComm* **2016**, *18*, 1645−1654.
(20) Watcharatharapong, T.; T-Thienprasert, J.; Barpanda, P.; Ahuja, R.; Chakraborty, S. Mechanistic Study of Na-Ion Diffusion and Small Polaron Formation in Kröhnkite $Na_2Fe(SO_4)_2{\cdot}2H_2O$ Based Cathode Materials. *J. Mater. Chem. A* **2017**, *5*, 21726−21739.
(21) Reynaud, M.; Rousse, G.; Abakumov, A. M.; Sougrati, M. T.; Van Tendeloo, G.; Chotard, J.-N.; Tarascon, J.-M. Design of New Electrode Materials for Li-Ion and Na-Ion Batteries from the Bloedite Mineral $Na_2Mg(SO_4)_2{\cdot}4H_2O$. *J. Mater. Chem. A* **2014**, *2*, 2671−2680.
(22) Marinova, D. M.; Zhecheva, E. N.; Kukeva, R. R.; Markov, P. V.; Nihtianova, D. D.; Stoyanova, R. K. Mixed Sodium Nickel-Manganese Sulfates: Crystal Structure Relationships between Hydrates and Anhydrous Salts. *J. Solid State Chem.* **2017**, *250*, 49−59.
(23) Saha, D.; Madras, G.; Guru Row, T. N. Manipulation of the Hydration Levels in Minerals of Sodium Cadmium Bisulfate toward the Design of Functional Materials. *Cryst. Growth Des.* **2011**, *11*, 3213−3221.
(24) Marinova, D.; Kostov, V.; Nikolova, R.; Kukeva, R.; Zhecheva, E.; Sendova-Vasileva, M.; Stoyanova, R. From Kröhnkite- to Alluaudite-Type of Structure: Novel Method of Synthesis of Sodium Manganese Sulfates with Electrochemical Properties in Alkali-Metal Ion Batteries. *J. Mater. Chem. A* **2015**, *3*, 22287−22299.
(25) Gavryushkin, P. N.; Thomas, V. G.; Bolotina, N. B.; Bakakin, V. V.; Golovin, A. V.; Seryotkin, Y. V.; Fursenko, D. A.; Litasov, K. D. Hydrothermal Synthesis and Structure Solution of $Na_2Ca(CO_3)_2$: "Synthetic Analogue" of Mineral Nyerereite. *Cryst. Growth Des.* **2016**, *16*, 1893−1902.
(26) Kovrugin, V. M.; Siidra, O. I.; Colmont, M.; Mentré, O.; Krivovichev, S. V. Emulating Exhalative Chemistry: Synthesis and Structural Characterization of Ilinskite, $Na[Cu_5O_2](SeO_3)_2Cl_3$, and Its K-Analogue. *Mineral. Petrol.* **2015**, *109*, 421−430.
(27) Skofteland, B. M.; Ellestad, O. H.; Lillerud, K. P. Potassium Merlinoite: Crystallization, Structural and Thermal Properties. *Microporous Mesoporous Mater.* **2001**, *43*, 61−71.
(28) Siidra, O. I.; Lukina, E. A.; Nazarchuk, E. V.; Depmeier, W.; Bubnova, R. S.; Agakhanov, A. A.; Avdontseva, E. Y.; Filatov, S. K.; Kovrugin, V. M. Saranchinaite, $Na_2Cu(SO_4)_2$, a New Exhalative Mineral from Tolbachik Volcano, Kamchatka, Russia, and a Product of the Reversible Dehydration of Kröhnkite, $Na_2Cu(SO_4)_2(H_2O)_2$. *Mineral. Mag.* **2018**, *82*, 257−274.
(29) Kovrugin, V. M.; Colmont, M.; Siidra, O. I.; Mentré, O.; Al-Shuray, A.; Gurzhiy, V. V.; Krivovichev, S. V. Oxocentered Cu(ii) Lead Selenite Honeycomb Lattices Hosting $Cu(i)Cl_2$ Groups Obtained by Chemical Vapor Transport Reactions. *Chem. Commun.* **2015**, *51*, 9563−9566.
(30) Kovrugin, V. M.; Colmont, M.; Siidra, O. I.; Gurzhiy, V. V.; Krivovichev, S. V.; Mentré, O. Pathways for Synthesis of New Selenium-Containing Oxo-Compounds: Chemical Vapor Transport Reactions, Hydrothermal Techniques and Evaporation Method. *J. Cryst. Growth* **2017**, *457*, 307−313.
(31) Sheldrick, G. M. Crystal Structure Refinement with SHELXL. *Acta Crystallogr., Sect. C: Struct. Chem.* **2015**, *C71*, 3−8.
(32) Petříček, V.; Dušek, M.; Palatinus, L. Crystallographic Computing System JANA2006: General Features. *Z. Kristallogr. - Cryst. Mater.* **2014**, *229*, 345−352.
(33) Berger, J. Infrared and Raman Spectra of $CuSO_4$, $5H_2O$; $CuSO_4$, $5D_2O$; and $CuSeO_4$, $5H_2O$. *J. Raman Spectrosc.* **1976**, *5*, 103−114.
(34) Hezel, A.; Ross, S. D. Forbidden Transitions in the Infra-Red Spectra of Tetrahedral Anions—III. Spectra-Structure Correlations in Perchlorates, Sulphates and Phosphates of the Formula MXO_4. *Spectrochim. Acta* **1966**, *22*, 1949−1961.
(35) Takahashi, H.; Meshitsuka, S.; Higasi, K. Infrared Spectra and Lattice Vibrations of Alkali and Alkaline—earth Metal Sulfates. *Spectrochim. Acta Part A Mol. Spectrosc.* **1975**, *31*, 1617−1622.
(36) Ross, S. D. Forbidden Transitions in the Infra-Red Spectra of Some Terahedral Anions—II. Sulphates. *Spectrochim. Acta* **1962**, *18*, 1575−1578.
(37) Decius, J. C.; Coker, E. H.; Brenna, G. L. The Vibrational Spectra of Sulfate Ions in Alkali Halide Crystals. *Spectrochim. Acta* **1963**, *19*, 1281−1289.
(38) Bakhtiari, F.; Darezereshki, E. One-Step Synthesis of Tenorite (CuO) Nano-Particles from $Cu_4(SO_4)(OH)_6$ by Direct Thermal-Decomposition Method. *Mater. Lett.* **2011**, *65*, 171−174.
(39) Usoltseva, N.; Korobochkin, V.; Dolinina, A. S.; Ustyugov, A. M. Infrared Spectra Investigation of CuO-Al_2O_3 Precursors Produced by Electrochemical Oxidation of Copper and Aluminum Using Alternating Current. *Key Eng. Mater.* **2016**, *712*, 65−70.
(40) Siidra, O. I.; Nazarchuk, E. V.; Zaitsev, A. N.; Lukina, E. A.; Avdontseva, E. Y.; Vergasova, L. P.; Vlasenko, N. S.; Filatov, S. K.; Turner, R.; Karpov, G. A. Copper Oxosulphates from Fumaroles of Tolbachik Volcano: Puninite, $Na_2Cu_3O(SO_4)_3$ − a New Mineral Species and Structure Refinements of Kamchatkite and Alumoklyuchevskite. *Eur. J. Mineral.* **2017**, *29*, 499−510.
(41) Kurtz, S. K.; Perry, T. T. A Powder Technique for the Evaluation of Nonlinear Optical Materials. *J. Appl. Phys.* **1968**, *39*, 3798−3813.
(42) Weber, M. J. *Handbook of Optical Materials*; CRC Press: New York, 2003.

(43) Burns, P. C.; Hawthorne, F. C. Coordination-Geometry Structural Pathways in Cu^{2+} Oxysalt Minerals. *Can. Mineral.* **1995**, *33*, 889−905.
(44) Yoshiasa, A.; Yagyu, G.; Ito, T.; Yamanaka, T.; Nagai, T. Crystal Structure of the High Pressure Phase(II) in $CuGeO_3$. *Z. Anorg. Allg. Chem.* **2000**, *626*, 36−41.
(45) Nadeem, M. A.; Bhadbhade, M.; Bircher, R.; Stride, J. A. Three Isolated Structural Motifs in One Crystal: Penetration of Two 1D Chains through Large Cavities within 2D Polymeric Sheets. *CrystEngComm* **2010**, *12*, 1391−1393.
(46) Schmidt, P.; Binnewies, M.; Glaum, R.; Schmidt, M. In Chemical Vapor Transport Reactions−Methods, Materials, Modeling. In *Advanced Topics on Crystal Growth*; Ferreira, S., Ed.; InTech: 2013; pp 227−305.
(47) Dwibedi, D.; Gond, R.; Dayamani, A.; Araujo, R. B.; Chakraborty, S.; Ahuja, R.; Barpanda, P. $Na_{2.32}Co_{1.84}(SO_4)_3$ as a New Member of the Alluaudite Family of High-Voltage Sodium Battery Cathodes. *Dalt. Trans.* **2017**, *46*, 55−63.
(48) Goñi, A.; Iturrondobeitia, A.; Gil de Muro, I.; Lezama, L.; Rojo, T. $Na_{2.5}Fe_{1.75}(SO_4)_3$ /Ketjen/RGO: An Advanced Cathode Composite for Sodium Ion Batteries. *J. Power Sources* **2017**, *369*, 95−102.
(49) Fehrmann, R.; Boghosian, S.; Papatheodorou, G. N.; Nielsen, K.; Berg, R. W.; Bjerrum, N. J.; Underhill, A. E. The Crystal Structure of $NaV(SO_4)_2$. *Acta Chem. Scand.* **1991**, *45*, 961−964.
(50) Boghosian, S.; Fehrmann, R.; Nielsen, K.; Liptay, G.; Snoeck, R.; Balzarini, J.; Fransson, B.; Ragnarsson, U.; Francis, G. W. Synthesis and Crystal Structure of $Na_3V(SO_4)_3$. Spectroscopic Characterization of $Na_3V(SO_4)_3$ and $NaV(SO_4)_2$. *Acta Chem. Scand.* **1994**, *48*, 724−731.
(51) Nielsen, K.; Boghosian, S.; Fehrmann, R.; Berg, R. W.; Ramondo, F.; Møller, J.; Senning, A.; Yao, X.-K.; Wang, H.-G.; Tuchagues, J.-P.; et al. Crystal Structure and Spectroscopic Characterization of a Green V(IV) Compound, $Na_8(VO)_2(SO_4)_6$. *Acta Chem. Scand.* **1999**, *53*, 15−23.
(52) Fehrmann, R.; Boghosian, S.; Papatheodorou, G. N.; Nielsen, K.; Berg, R. W.; Bjerrum, N. J. Crystal Structure and Vibrational Spectra of $Na_2VO(SO_4)_2$. *Inorg. Chem.* **1990**, *29*, 3294−3298.
(53) Amann, P.; Möller, A. Reactivity, Syntheses, and Crystal Structures of $Na_5[MO_2][X]$ with M = Co^+, Ni^+, Cu^+; X = CO_3^{2-}, SO_4^{2-}, SO_3^{2-}, S^{2-}, and $Na_{25}[CuO_2]_5[SO_4]_4[S]$. *Z. Anorg. Allg. Chem.* **2003**, *629*, 1643−1650.
(54) Amann, P.; Kataev, V.; Möller, A. Synthesis and Characterization of $Na_{11}[CuO_4][SO_4]_3$. *J. Solid State Chem.* **2004**, *177*, 2889−2895.
(55) Möller, A.; Sobotka, B. M.; Baier, J.; Freimuth, A. Ein Natrium-Oxocobaltat(II)-Sulfat: $Na_8[CoO_3][SO_4]_2$. *Z. Anorg. Allg. Chem.* **2002**, *628*, 2705−2708.
(56) Schäffer, S. J. C.; Berg, R. W. Catena-Poly[Tetrasodium [[Cis-Dioxido-Trans-Bis(Sulfato-KO)Molybdate(VI)]-μ-Sulfato-K2O:O′]]. *Acta Crystallogr., Sect. E: Struct. Rep. Online* **2008**, *E64*, i73−i73.
(57) Scordari, F.; Ventruti, G.; Gualtieri, A. F.; Lausi, A. Crystal Structure of $Na_3Fe(SO_4)_3$: A High-Temperature Product (400 C) of Sideronatrite $[Na_2Fe(SO_4)_2OH{\cdot}3H_2O]$. *Am. Mineral.* **2011**, *96*, 1107−1111.
(58) Driscoll, L. L.; Kendrick, E.; Wright, A. J.; Slater, P. R. Investigation into the Effect on Structure of Oxoanion Doping in $Na_2M(SO_4)_2{\cdot}2H_2O$. *J. Solid State Chem.* **2016**, *242*, 103−111.
(59) Shannon, R. D. Revised Effective Ionic Radii and Systematic Studies of Interatomic Distances in Halides and Chalcogenides. *Acta Crystallogr., Sect. A: Cryst. Phys., Diffr., Theor. Gen. Crystallogr.* **1976**, *A32*, 751−767.
(60) Varughese, S.; Desiraju, G. R. Using Water as a Design Element in Crystal Engineering. Host−Guest Compounds of Hydrated 3,5-Dihydroxybenzoic Acid. *Cryst. Growth Des.* **2010**, *10*, 4184−4196.
(61) Driscoll, L. L.; Kendrick, E.; Knight, K. S.; Wright, A. J.; Slater, P. R. Investigation into the Dehydration of Selenate Doped $Na_2M(SO_4)_2{\cdot}2H_2O$ (M = Mn, Fe, Co and Ni): Stabilisation of the High Na Content Alluaudite Phases $Na_3M_{1.5}(SO_4)_{3-1.5x}(SeO_4)_{1.5x}$ (M = Mn, Co and Ni) through Selenate Incorporation. *J. Solid State Chem.* **2018**, *258*, 64−71.
(62) Alonso, J. A.; Martínez-Lope, M. J.; Casais, M. T.; Fernández-Díaz, M. T. Evolution of the Jahn−Teller Distortion of MnO_6 Octahedra in $RMnO_3$ Perovskites (R = Pr, Nd, Dy, Tb, Ho, Er, Y): A Neutron Diffraction Study. *Inorg. Chem.* **2000**, *39*, 917−923.
(63) Siidra, O. I.; Nazarchuk, E. V.; Agakhanov, A. A.; Lukina, E. A.; Zaitsev, A. N.; Turner, R.; Filatov, S. K.; Pekov, I. V.; Karpov, G. A.; Yapaskurt, V. O. Hermannjahnite, $CuZn(SO_4)_2$, a New Mineral with Chalcocyanite Derivative Structure from the Naboko Scoria Cone of the 2012−2013 Fissure Eruption at Tolbachik Volcano, Kamchatka, Russia. *Mineral. Petrol.* **2018**, *112*, 123−134.
(64) Kovrugin, V. M.; Colmont, M.; Siidra, O. I.; Charkin, D. O.; Aliev, A.; Krivovichev, S. V.; Mentré, O. Synthesis and Structural Variety of First Mn and Bi Selenites and Selenite Chlorides. *Z. Kristallogr. - Cryst. Mater.* **2018**, DOI: 10.1515/zkri-2018-2088.
(65) Krivovichev, S. V. Structural Complexity of Minerals: Information Storage and Processing in the Mineral World. *Mineral. Mag.* **2013**, *77*, 275−326.
(66) Krivovichev, S. V. Topological Complexity of Crystal Structures: Quantitative Approach. *Acta Crystallogr., Sect. A: Found. Crystallogr.* **2012**, *A68*, 393−398.
(67) Krivovichev, S. V. Ladders of Information: What Contributes to the Structural Complexity of Inorganic Crystals. *Z. Kristallogr. - Cryst. Mater.* **2018**, *233*, 155−161.
(68) Blatov, V. A.; Shevchenko, A. P.; Proserpio, D. M. Applied Topological Analysis of Crystal Structures with the Program Package ToposPro. *Cryst. Growth Des.* **2014**, *14*, 3576−3586.
(69) Krivovichev, S. V. Which Inorganic Structures Are the Most Complex? *Angew. Chem., Int. Ed.* **2014**, *53*, 654−661.
(70) Sun, M.; Rousse, G.; Abakumov, A. M.; Saubanère, M.; Doublet, M.-L.; Rodríguez-Carvajal, J.; Van Tendeloo, G.; Tarascon, J.-M. $Li_2Cu_2O(SO_4)_2$: A Possible Electrode for Sustainable Li-Based Batteries Showing a 4.7 V Redox Activity vs Li^+/Li^0. *Chem. Mater.* **2015**, *27*, 3077−3087.
(71) Lander, L.; Rousse, G.; Batuk, D.; Colin, C. V.; Dalla Corte, D. A.; Tarascon, J.-M. Synthesis, Structure, and Electrochemical Properties of K-Based Sulfates $K_2M_2(SO_4)_3$ with M = Fe and Cu. *Inorg. Chem.* **2017**, *56*, 2013−2021.
(72) Rodríguez-Carvajal, J. Recent Advances in Magnetic Structure Determination by Neutron Powder Diffraction. *Phys. B* **1993**, *192*, 55−69.
(73) Boivin, E.; Chotard, J.-N.; Bamine, T.; Carlier, D.; Serras, P.; Palomares, V.; Rojo, T.; Iadecola, A.; Dupont, L.; Bourgeois, L.; et al. Vanadyl-Type Defects in Tavorite-like $NaVPO_4F$: From the Average Long Range Structure to Local Environments. *J. Mater. Chem. A* **2017**, *5*, 25044−25055.
(74) Kovrugin, V. M.; David, R.; Chotard, J.-N.; Recham, N.; Masquelier, C. A High Voltage Cathode Material for Sodium Batteries: $Na_3V(PO_4)_2$. *Inorg. Chem.* **2018**, *57*, 8760−8768.
(75) Bleaney, B.; Bowers, K. D. Anomalous Paramagnetism of Copper Acetate. *Proc. R. Soc. A Math. Phys. Eng. Sci.* **1952**, *214*, 451−465.
(76) Krivovichev, S. V. In *Minerals as Advanced Materials I*; Krivovichev, S. V., Ed.; Springer Berlin Heidelberg: Berlin, Heidelberg, 2008.
(77) Cundy, C. S.; Cox, P. A. The Hydrothermal Synthesis of Zeolites: Precursors, Intermediates and Reaction Mechanism. *Microporous Mesoporous Mater.* **2005**, *82*, 1−78.
(78) Swain, D.; Guru Row, T. N. In Situ Phase Separation Following Dehydration in Bimetallic Sulfates: A Variable-Temperature X-Ray Diffraction Study. *Inorg. Chem.* **2009**, *48*, 7048−7058.
(79) Fry, A. M.; Sweeney, O. T.; Adam Phelan, W.; Drichko, N.; Siegler, M. A.; McQueen, T. M. Unique Edge-Sharing Sulfate-Transition Metal Coordination in $Na_2M(SO_4)_2$ (M = Ni and Co). *J. Solid State Chem.* **2015**, *222*, 129−135.
(80) Berg, R. W.; Thorup, N. The Reaction between ZnO and Molten $Na_2S_2O_7$ or $K_2S_2O_7$ Forming $Na_2Zn(SO_4)_2$ or $K_2Zn(SO_4)_2$,

Studied by Raman Spectroscopy and X-Ray Diffraction. *Inorg. Chem.* **2005**, *44*, 3485−3493.
(81) Swain, D.; Guru Row, T. N. Structure, Ionic Conduction and Dielectric Relaxation in a Novel Fast Ion Conductor, $Na_2Cd(SO_4)_2$. *Chem. Mater.* **2007**, *19*, 347−349.
(82) Pradhan, G. K.; Swain, D.; Guru Row, T. N.; Narayana, C. High-Temperature Phase Transition Studies in a Novel Fast Ion Conductor, $Na_2Cd(SO_4)_2$, Probed by Raman Spectroscopy. *J. Phys. Chem. A* **2009**, *113*, 1505−1507.
(83) Wildner, M.; Stoilova, D. Crystal Structures and Crystal Chemical Relationships of Kröhnkite- and Collinsite-Type Compounds $Na_2Me^{2+}(XO_4)_2{\cdot}2H_2O$ (X = S, Me = Mn, Cd; and X = Se, Me = Mn, Co, Ni, Zn, Cd) and $K_2Co(SeO_4)_2{\cdot}2H_2O$. *Zeitschrift für Krist. - Cryst. Mater.* **2003**, *218*, 201−209.
(84) Stoilova, D.; Wildner, M.; Koleva, V. Vibrational Behavior of the S-O Stretches in Compounds with Kröhnkite-Type Chains $Na_2Me(SeO_4)_2{\cdot}2H_2O$ with Matrix-Isolated SO_4^{2-} and Me'^{2+} Guest Ions (Me = Mn, Co, Ni, Cu, Zn, Cd). *Vib. Spectrosc.* **2003**, *31*, 115−123.
(85) Hawthorne, F. C.; Ferguson, R. B. Refinement of the Crystal Structure of Kröhnkite. *Acta Crystallogr., Sect. B: Struct. Crystallogr. Cryst. Chem.* **1975**, *B31*, 1753−1755.
(86) Rao, B. R. Die Verfeinerung Der Kristallstruktur von Kröhnkit, $Na_2Cu(SO_4)_2{\cdot}2H_2O$. *Acta Crystallogr.* **1961**, *14*, 738−743.
(87) Onac, B.; Effenberger, H.; Collins, N.; Kearns, J.; Breban, R. Revisiting Three Minerals from Cioclovina Cave (Romania). *Int. J. Speleol.* **2011**, *40*, 99−108.
(88) Hudák, M.; Díaz, J. G.; Kožíšek, J. Disodium Tetraaquabis(Sulfato)Iron(II). *Acta Crystallogr., Sect. E: Struct. Rep. Online* **2008**, *E64*, i10−i10.
(89) Stoilova, D.; Wildner, M. Blödite-Type Compounds $Na_2Me(SO_4)_2{\cdot}4H_2O$ (Me = Mg, Co, Ni, Zn): Crystal Structures and Hydrogen Bonding Systems. *J. Mol. Struct.* **2004**, *706*, 57−63.
(90) Bukin, V. I.; Nozik, Y. Z. Neutron Diffraction Study of the Crystal Structure of Cobalt Astrakhanite $Na_2Co(SO_4)_2{\cdot}4H_2O$. *Sov. Phys. Crystallogr.* **1975**, *20*, 180−182.
(91) Díaz de Vivar, M. E.; Baggio, S.; Garland, M. T.; Baggio, R. Disodium Nickel Bis(Sulfate) Tetrahydrate: A Nickel Astrakanite. *Acta Crystallogr., Sect. E: Struct. Rep. Online* **2006**, *E62*, i196−i198.
(92) Díaz de Vivar, M. E.; Baggio, S.; Ibáñez, A.; Baggio, R. Disodium Zinc Bis(Sulfate) Tetrahydrate (Zinc Astrakanite) Revisited. *Acta Crystallogr., Sect. E: Struct. Rep. Online* **2008**, *E64*, i30−i31.
(93) Giglio, M. Die Kristallstruktur von $Na_2Zn(SO_4)_2{\cdot}4H_2O$ (Zn-Blödit). *Acta Crystallogr.* **1958**, *11*, 789−794.
(94) Bukin, V. I.; Nozik, Y. Z. A Neutronographic Investigation of Hydrogen Bonding in Zinc Astrakanite $Na_2Zn(SO_4)_2(H_2O)_4$. *J. Struct. Chem.* **1974**, *15*, 616−619.
(95) Yaokang, L.; Yunlong, F. Crystal Structure and Properties of a New Tutton Salt $Na_2[Co(H_2O)_6](SO_4)_2$. *Chin. J. Chem.* **2009**, *25*, 447−453.
(96) Zhao, P. S.; Jian, F. F.; Bai, Z. S.; Zheng, J.; Zhuang, R. R. Hydrothermal Synthesis, Structure and Thermal Property of a 2-Dimensional Network: Sodium Sulfate $[Ni(H_2O)_6(NaSO_4)_2]$. *Struct. Chem.* **2006**, *17*, 519−523.
(97) Wu, W.; Xie, J.-M.; Xie, D.-P.; Xuan, Y.-W. Poly-[Hexaaquacopper(II) [Di-M3-Sulfato-Disodiate(I)]]. *Acta Crystallogr., Sect. E: Struct. Rep. Online* **2008**, *E64*, i7−i7.